remote sensing

MDPI

Article

Dual Receiver EGNOS+SDCM Positioning with C1C and C1W Pseudo-Range Measurements

Mieczysław Bakuła [1,*], Kamil Krasuski [1] and Karol Dawidowicz [2]

[1] Institute of Navigation, Polish Air Force University, 08-521 Dęblin, Poland; k.krasuski@law.mil.pl
[2] Institute of Geodesy and Civil Engineering, University of Warmia and Mazury, 10-724 Olsztyn, Poland; karol.dawidowicz@uwm.edu.pl
* Correspondence: m.bakula@law.mil.pl

Abstract: The paper presents an approach to the simultaneous use of SDCM and EGNOS corrections for two GNSS receivers placed at a constant distance. The SDCM and EGNOS corrections were applied for two GPS code measurements on L1 frequency: C1C and C1W. The approach is based mainly on the constrained least squares adjustment, but for the horizontal and vertical coordinates, the Kalman Filter was applied in order to reduce pseudo-range noises. It allows for obtaining a higher autonomous accuracy of GPS/(SDCM+EGNOS) positioning than when using only the GPS/EGNOS or GPS/SDCM system. The final dual-redundant solution, in which two SBAS systems were used (EGNOS+SDCM) and two GPS pseudo-ranges (C1C+C1W) were present, yielded RMS errors of 0.11 m for the horizontal coordinates and 0.25 m for the vertical coordinates. Moreover, the accuracy analysis in the developed mathematical model for the determined 3D coordinates with simultaneous use of EGNOS and SDCM systems proved to be much more reliable than using only a single EGNOS or SDCM system. The presented approach can be used not only for precise navigation, but also for some geoscience applications and remote sensing where the reliable accuracy of autonomous GPS positioning is required.

Keywords: SBAS positioning; EGNOS; SDCM; differential GPS; least squares adjustment; Kalman filtering; pseudo-range measurements

check for updates

Citation: Bakuła, M.; Krasuski, K.; Dawidowicz, K. Dual Receiver EGNOS+SDCM Positioning with C1C and C1W Pseudo-Range Measurements. *Remote Sens.* **2022**, *14*, 3152. https://doi.org/10.3390/rs14133152

Academic Editor: Xiaogong Hu

Received: 27 May 2022
Accepted: 27 June 2022
Published: 30 June 2022

Publisher's Note: MDPI stays neutral with regard to jurisdictional claims in published maps and institutional affiliations.

Copyright: © 2022 by the authors. Licensee MDPI, Basel, Switzerland. This article is an open access article distributed under the terms and conditions of the Creative Commons Attribution (CC BY) license (https://creativecommons.org/licenses/by/4.0/).

1. Introduction

GNSS positioning is an efficient tool for various geoscience surveys in kinematic and static positioning. Numerous different methods are currently used in practice for various geoscience applications, e.g., static or rapid-static surveying, differential code or phase positioning, modern Precise Point Positioning (PPP) technology, as well as the RTK (Real-Time Kinematic) method. Most modern GNSS technologies are based on permanent reference stations that are commonly used in many countries. Permanent reference stations can reduce distance-dependent errors in the carrier and pseudo-range measurements at the user station [1]. The accuracy for a longer baseline length can be improved if a ground reference station is used. Distance-dependent errors affect integrity performance, which is important for safety-critical applications, such as aircraft approaching and landing [2]. In field measurements using only one mobile GNSS receiver, there is always the probability of making gross errors, particularly if the measurement is taken under difficult observation conditions [3,4], at a large distance from the reference station or during a period of high atmospheric activity [5,6]. Although GNSS technology is applied mainly for static measurements, it may also be effectively used for various kinematic positioning and remote sensing applications, e.g., in remote sensing and mobile mapping LIDAR systems [7,8] where cm accuracy is required, precise land GNSS navigation [9,10], as well as for UAV precise mapping systems [8] and UAV photogrammetry [11]. In static GNSS positioning, each measurement epoch provides redundant observations (coordinates) or redundant

GNSS baselines [3,4,12]. In kinematic GNSS positioning at a given time and for a given position, just a single solution is obtained. Therefore, there are no redundant coordinates for a rover GNSS receiver [13,14]. A solution to improve the control of GNSS results may be a measurement using more than one rover GNSS receiver, which simultaneously determines its position [15–19] or uses multi-baselines from permanent reference stations [20–22], or the integration of both approaches [23,24] where multi-baselines and multi-rover receivers are used for precise and reliable GNSS positioning. In GNSS surveying, we expect cm or even mm accuracy. However, in navigation, meter or decimetre accuracy is sufficient for many processes; therefore, it is not always necessary to use precise phase observations. For GNSS navigation, SBAS autonomous systems are used, mainly those that employ code observations. The absolute positioning technique is based on a point positioning mode with a single Global Navigation Satellite System (GNSS) receiver. For a long period, this positioning technique has relied mainly on a single GPS system. Autonomous GPS Standard Point Positioning (SPP) is not satisfying in terms of the accuracy and integrity for demanding safety of life applications [25], especially if we use only the GPS system. To improve these, the Satellite-Based Augmentation Systems (SBAS) were created in some parts of the world, e.g., in the USA (WAAS—Wide Area Augmentation System) [25–28], Japan (MTSAT—Satellite-Based Augmentation System-MSAS) [29], India (GAGAN—GEO Augmented Navigation System), Europe (EGNOS—European Geostationary Navigation Overlay Service), Russia (SDCM—System of Differential Correction and Monitoring), and China's BeiDou SBAS (BDSBAS) [30]. A multi-constellation GNSS increases the robustness against the potential degradation of core satellite constellations and extends the service coverage area [31]. The SBAS systems broadcast corrections related to satellite positions and clocks and tropospheric and ionospheric corrections. These corrections are transmitted to the users via geostationary satellites. EGNOS is one of the SBAS systems that supports GPS operation [32]. Although SDCM is a Russian system, it also generates corrections for GPS systems. SDCM GPS corrections are transmitted by the geostationary satellites: PRN 125, PRN 140, and PRN 141. The first results of the Russian System for Differential Corrections and Monitoring (SDCM) were presented by Averin et al. [33,34]. The SDCM system was then under development since 2002, and in 2006, part of it was put into operation. The coverage of the system is the territory of the Russian Federation. The positioning accuracy of GPS/EGNOS positioning in central Europe showed that the horizontal accuracy of a single EGNOS receiver is in the range of 0.5–2.5 m and the vertical one is 1.5–3.0 m [35–40]. The current EGNOS performance was presented in the latest release of The European GNSS Agency document of 2019 [41]. The positioning accuracy in this document is determined by the 3 m (95%) in the horizontal plane and 4 m (95%) in the vertical plane. These values are established for the whole area covered by the operation of EGNOS. Therefore, EGNOS may be used in aviation [42–45], mobile mapping and remote sensing, maritime, rail and road, archaeology, geosciences, and more. In a multi-GNSS receiver, more than one GNSS system is used to increase the accuracy and reliability of the SBAS position [46–49]. Many studies have already analysed the modifications of standard solutions based on SBAS systems. The findings on improving the integrity and availability of SBAS positioning are reported in [50,51].

The authors of the referenced articles on SBAS/GPS positioning only used the C1C code, which is the base code at L1 = 1575.42 MHz frequency. However, on the L1 frequency, there is also the C1W code [52], which can also be used to determine a position, taking EGNOS corrections into account. Some fundamental information on code observations has been described by, e.g., Kaplan [53]. Therefore, such research seems to be justified. Additionally, a second GNSS receiver was used to increase accuracy and reliability. When placed at a fixed distance, it allows independent control and facilitates the determination of accuracy using the constrained least squares (LS) adjustment method. Due to the noise of the code measurements, a Kalman filter was used to complete the least squares method. Thus, the measurement of the GNSS set should consist of two rover GNSS receivers set at a fixed distance from each other. The unknown point (P) is located between receivers

R1 and R2. Relatively fixed distances between rover receivers improve the accuracy and reliability of GPS positioning, which is indispensable in applications dedicated for air navigation. The SBAS positioning calculations have been presented for EGNOS and SDCM, as well as for EGNOS+SDCM. The SBAS calculations were performed for the C1C and C1W code solutions at the L1 GPS frequency. The research was carried out using two Javad TRIUMPH-1 GNSS receivers. EGNOS and SDCM corrections were included in GPS code observations, using RTKLIB Software version 2.4.3 b34 [54] (http://rtklib.com/, accessed on 1 February 2022; the software created by Takasu Tomoji, Tokyo, Japan). The stages of data processing can be presented as a diagram (Figure 1). The measurement and calculation process of dual-redundant GPS/SBAS positioning consists of five steps:

I. Taking measurements with C1C and C1W codes using two independent GPS receivers.
II. A determination of the EGNOS and SDCM autonomous position for single measurement epochs, for C1C and C1W code solutions, using the least squares method.
III. The use of Kalman filtering to smoothen the coordinates obtained in step II.
IV. Using a forced equation with a known 3D distance between two GNSS receivers.
V. Conducting an accuracy analysis of the obtained coordinates using the least squares covariance matrix adjustment solution.

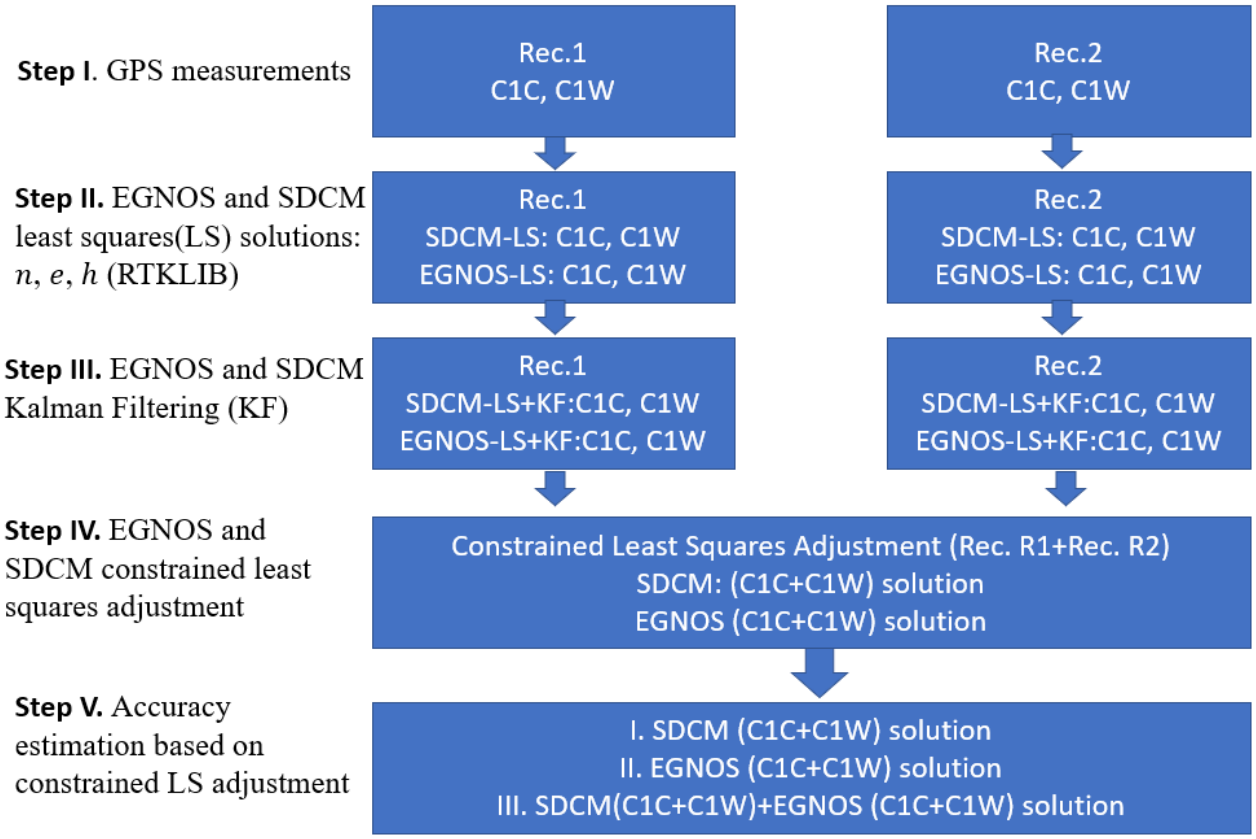


Figure 1. Diagram of double receiver EGNOS+SDCM positioning.

Sections 2 and 3 of the contribution outline the details of the mathematical models. In Section 4, experiments and analyses of the methodology are given. Section 5 presents the accuracy analysis of the method constrained least squares adjustment for the systems: EGNOS, SDCM, and EGNOS+SDCM. The concluding remarks are presented in Section 6.

2. Kalman Filtering in SBAS Positioning

The Kalman filter provides a sequential and recursive algorithm for the optimal linear minimum variance of error estimation of the system state, x_k, based on the set of measurements, $y_1, \ldots\ y_k$, for systems described by a linear state-space model [55]:

$$x_{k+1} = \Phi_k x_k + w_k \tag{1}$$

$$y_k = H_k x_k + v_k \tag{2}$$

with the auto and cross covariance functions of w_k and v_k that can be expressed as:

$$E\left[w_k, w_l^T\right] = \begin{cases} Q_k, & k = l \\ 0, & k \neq l \end{cases} \tag{3}$$

$$E\left[v_k, v_l^T\right] = \begin{cases} R_k, & k = l \\ 0, & k \neq l \end{cases}, \tag{4}$$

$$E\left[w_k, v_l^T\right] = 0 \text{ for all } k,\ l \tag{5}$$

where:

Φ_k—is the state transition matrix;
H_k—is the matrix giving the relationship between y_k and x_k when no noise is present;
x_k—is the state vector at time t_k;
w_k—is the process noise at time t_k;
v_k—is a measurement white noise vector at time t_k.

The derivation of the Kalman recursive filter equations can be found in [55]. A schematic of equations flow is summarised in Figure 2 [56,57].

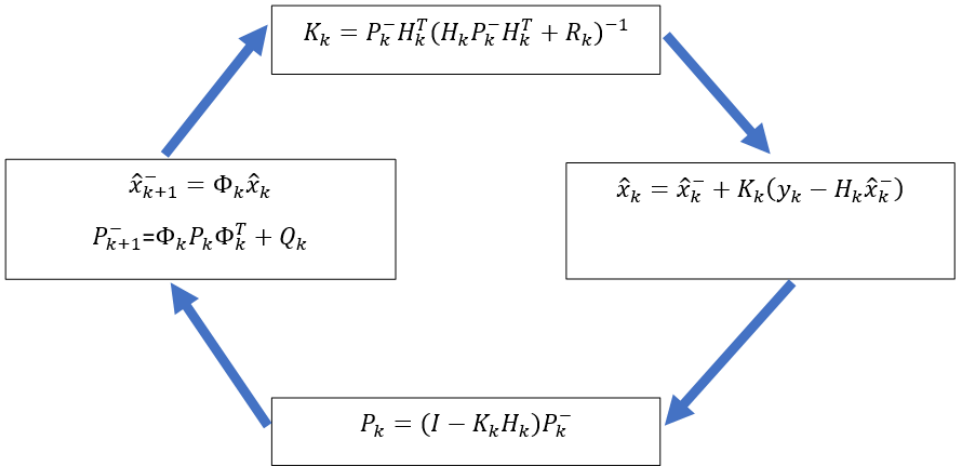


Figure 2. Flow diagram of the Kalman filter equations based on [56,57].

The observation equations expressed by Equation (1) are for the horizontal coordinates n, e and the vertical coordinate h, obtained from SBAS/EGNOS and SBAS/SDCM positioning. These coordinates may be derived from the least squares solution. In this study, Kalman filtering was additionally applied to horizontal and vertical coordinates, which had been earlier determined by SBAS positioning. Horizontal and vertical coordinates were considered as independent observations for two rover GNSS receivers. The value v_k, understood as the noise of the observation model, was assumed at the level of 1.75 m, which is related to the accuracy of the code positioning for the L1 frequency. It is important to adopt an appropriate w_k value, which determines the accuracy of the kinematic model.

For the purposes of this research project, the w_k value was set at 0.1 m. Based on the adopted observation model, the H_k, Φ_k, R_k, Q_k matrices are therefore equal, respectively:

$$H_k = diag(1\ \ 1\ \ 1) \tag{6}$$

$$\Phi_k = diag(1\ \ 1\ \ 1) \tag{7}$$

$$R_k = diag(3\ \ 3\ \ 3) \tag{8}$$

$$Q_k = diag(0.01\ \ 0.01\ \ 0.01) \tag{9}$$

while the y_k vector will contain observations (13), i.e.,

$$y_k = \begin{bmatrix} n \\ e \\ h \end{bmatrix} \tag{10}$$

The relationships between the z_k and x_k vectors are specified in Formulas (1) and (2), and are dependent on a priori acquired noise of the observation model (v_k) and noise of the kinematic model (w_k). Due to the fact that the GPS-SBAS positions carry a certain random error, the values n, e, h may vary slightly in successive time measurement spans and it will be difficult to make their proper estimates. Therefore, for the GPS/SBAS receiver, we used the Kalman filter in order to reduce random errors for the coordinates determined in successive time measurement spans. Horizontal coordinates represented Universal Transverse Mercator (UTM) coordinates (n–UTM Northing; e–UTM Easting) but h represented an ellipsoidal height in the Earth Cantered Earth Fixed (ECEF) coordinate system.

3. Mathematic Model of Dual Receiver in SBAS Positioning

In the fourth step of our approach, the constrained least squares adjustment is adopted. For the GNSS receivers presented in Figure 3, considering the coordinates being determined by the SBAS method based on two mobile receivers ($R1$, $R2$), for each component of the horizontal coordinates (n, e) and the vertical coordinate (h), we may write down the following observation equations:

$$\begin{cases} n_{R1} + v_{n,R1} = n^o_{R1} + dn_{R1} \\ e_{R1} + v_{e,R1} = e^o_{R1} + de_{R1} \\ h_{R1} + v_{h,R1} = h^o_{R1} + dh_{R1} \\ n_{R2} + v_{n,R2} = n^o_{R2} + dn_{R2} \\ e_{R2} + v_{e,R2} = e^o_{R2} + de_{R2} \\ h_{R2} + v_{h,R2} = h^o_{R2} + dh_{R2} \end{cases} \tag{11}$$

where the values n^o_{R1}, e^o_{R1}, h^o_{R1}, n^o_{R2}, e^o_{R2}, h^o_{R2} represent the approximated coordinates of points $R1$ and $R2$.



Figure 3. Javad TRIUMPH-1 receivers taking part in the experiment.

Following the simplification, in the matrix format, the system of adjustment equations may be presented as:

$$V = AX + L \tag{12}$$

or

$$\begin{bmatrix} v_{n,R1} \\ v_{e,R1} \\ v_{h,R1} \\ v_{n,R2} \\ v_{e,R2} \\ v_{h,R2} \end{bmatrix} = \begin{bmatrix} 1 & 0 & 0 & 0 & 0 & 0 \\ 0 & 1 & 0 & 0 & 0 & 0 \\ 0 & 0 & 1 & 0 & 0 & 0 \\ 0 & 0 & 0 & 1 & 0 & 0 \\ 0 & 0 & 0 & 0 & 1 & 0 \\ 0 & 0 & 0 & 0 & 0 & 1 \end{bmatrix} X + \begin{bmatrix} n^o_{R1} - n_{R1} \\ e^o_{R1} - e_{R1} \\ h^o_{R1} - h_{R1} \\ n^o_{R2} - n_{R2} \\ e^o_{R2} - e_{R2} \\ h^o_{R2} - h_{R2} \end{bmatrix}, \tag{13}$$

where $X^T = \begin{bmatrix} dn_{R1}, & de_{R1}, & dh_{R1}, dn_{R2}, & de_{R2}, & dh_{R2} \end{bmatrix}$ are the unknown parameters.

Given the fixed distance between receivers $R1 - R2$, and their fixed height, one may additionally write the conditional equation for the distance $R1 - R2$, considering the unknown parameters:

$$0 = D^o_{R1,R2} + dx - 0.5, \tag{14}$$

and the conditional equation for the height:

$$0 = h^o_{R2} + dh_{R2} - h^o_{R1} - dh_{R1} \tag{15}$$

where the expression $D^o_{R1,R2}$, represents the approximated spatial distance between receivers $R1$ and $R2$, computed from the formula:

$$D^o_{R1,R2} = \sqrt{\left(n^o_{R1} - n^o_{R2}\right)^2 + \left(e^o_{R1} - e^o_{R2}\right)^2 + \left(h^o_{R1} - h^o_{R2}\right)^2} \tag{16}$$

Given the fixed distance between receivers $R1 - R2$, and their fixed height, one may additionally write the conditional equation for the distance $R1 - R2$, considering the unknown parameters.

The observational value $D_{R1,R2}$ must be brought to the linear form by expanding the Taylor series. That is why the expression dx represents the partial derivatives on extension of the Taylor series:

$$\begin{aligned} dx = - & \frac{\left(n^o_{R1} - n^o_{R2}\right)}{D^o_{R1,R2}} dn_{R1} - \frac{\left(e^o_{R1} - e^o_{R2}\right)}{D^o_{R1,R2}} de_{R1} - \frac{\left(h^o_{R1} - h^o_{R2}\right)}{D^o_{R1,R2}} dh_{R1} \\ & + \frac{\left(n^o_{R1} - n^o_{R2}\right)}{D^o_{R1,R2}} dn_{R2} + \frac{\left(e^o_{R1} - e^o_{R2}\right)}{D^o_{R1,R2}} de_{R2} + \frac{\left(h^o_{R1} - h^o_{R2}\right)}{D^o_{R1,R2}} dh_{R2}. \end{aligned} \tag{17}$$

Additionally, the observational equation for the spatial distance in the matrix form with the conditional equation for the height may be written as:

$$A_w X + L_w = 0, \tag{18}$$

where for Figure 2, the matrices A_w and L_w are expressed as follows:

$$A_w = \begin{bmatrix} -\frac{\left(n^o_{R1} - n^o_{R2}\right)}{D^o_{R1,R2}} & -\frac{\left(e^o_{R1} - e^o_{R2}\right)}{D^o_{R1,R2}} & -\frac{\left(h^o_{R1} - h^o_{R2}\right)}{D^o_{R1,R2}} & \frac{\left(n^o_{R1} - n^o_{R2}\right)}{D^o_{R1,R2}} & \frac{\left(e^o_{R1} - e^o_{R2}\right)}{D^o_{R1,R2}} & \frac{\left(h^o_{R1} - h^o_{R2}\right)}{D^o_{R1,R2}} \\ 0 & 0 & -1 & 0 & 0 & 1 \end{bmatrix} \tag{19}$$

$$L_w = \begin{bmatrix} D^o_{R1,R2} - 0.5 \\ h^o_{R2} - h^o_{R1} \end{bmatrix}. \tag{20}$$

The above matrices apply to static measurements where two SBAS receivers are positioned at the same height. In the event of the SBAS receiver moving within the 3D space, the above equations are limited to just one condition, i.e.,: the spatial distance 3D between points $R1$ and $R2$, i.e.,:

$$A_w = \begin{bmatrix} -\frac{\left(n^o_{R1} - n^o_{R2}\right)}{D^o_{R1,R2}} & -\frac{\left(e^o_{R1} - e^o_{R2}\right)}{D^o_{R1,R2}} & -\frac{\left(h^o_{R1} - h^o_{R2}\right)}{D^o_{R1,R2}} & \frac{\left(n^o_{R1} - n^o_{R2}\right)}{D^o_{R1,R2}} & \frac{\left(e^o_{R1} - e^o_{R2}\right)}{D^o_{R1,R2}} & \frac{\left(h^o_{R1} - h^o_{R2}\right)}{D^o_{R1,R2}} \end{bmatrix} \tag{21}$$

$$L_w = \begin{bmatrix} D^o_{R1,R2} - 0.5 \end{bmatrix}. \tag{22}$$

Next, combining the observational equations with geometric conditions, the following linear system of equations is obtained [56]:

$$\begin{cases} AX + L = V \\ A_w X + L_w = 0 \end{cases} \tag{23}$$

Determination of the vector of the unknown X, which satisfies the above equations, is performed by minimising the Lagrange function:

$$\psi(X) = V^T P_L V + 2K^T (A_w X + L_w), \tag{24}$$

where K is the Lagrange's unknown multiplier vector [56].

After determining the derivative $\psi(X)$ in relation to X and the equation to zero, the final solution may be noted in the format [58,59]:

$$\begin{cases} A^T P_L A X + {A_w}^T K + A^T P_L L = 0 \\ A_w X + L_w = 0 \end{cases} \tag{25}$$

and hence, the final solution is equal to:

$$\begin{bmatrix} X \\ K \end{bmatrix} = \begin{bmatrix} A^T P_L A & {A_w}^T \\ A_w & 0 \end{bmatrix}^{-1} \begin{bmatrix} A^T P_L L \\ L_w \end{bmatrix}, \tag{26}$$

which is a convenient format for programming in the Matlab environment.

Two GPS/SBAS receivers positioned at equal distances from the main point participate in the presented measurement method and thus the coordinates of the main point (n_P, e_P, h_P) are computed as the arithmetic average:

$$\begin{bmatrix} n_P \\ e_P \\ h_P \end{bmatrix} = 2^{-1} \begin{bmatrix} n_{R1} + n_{R2} \\ e_{R1} + e_{R2} \\ h_{R1} + h_{R2} \end{bmatrix}. \tag{27}$$

4. Experimental Test and Results

The GNSS test measurements were made using two Javad TRIUMPH-1 receivers on 30 October 2020, at 9:10:00–9:43:19 UTC, with a one-second measurement interval. The configuration of the GNSS satellites during the measurement is shown in Figure 4. The GNSS receivers (R1 and R2) recorded code and phase observations, which were saved to *.jps type files. Next, using Javad's JPS2RIN software, each binary *.jps file was converted to RINEX ver. 3.00 GPS-only format in such a manner that the RINEX GPS file contained C1C or C1W code observations. Therefore, for each *.jps file, two RINEX GPS files were obtained, respectively: for R1.jps: R1-C1C.20o and R1-C1W.20o; and for R2.jps: R2-C1C.20o and R2-C1W.20o. Next, for receivers R1 and R2, and four files in RINEX format, SBAS positioning calculations were performed, using EGNOS correction and SDCM using RTKLIB ver. 2.4.3 b34 [54]. The calculations were performed for GPS satellites with an elevation of more than 5 degrees. The results of these calculations for the horizontal and vertical coordinates are depicted in Figures 5–8. The SBAS positioning results for the C1C code are presented in Figures 5 and 6, while for the C1W code observations, the results are to be found in Figures 7 and 8. The accuracy of the obtained positions equalled approximately 0.5–1.5 m. The average RMS errors for the plane coordinates (n, e) and the vertical coordinate (h) are shown in Table 1.

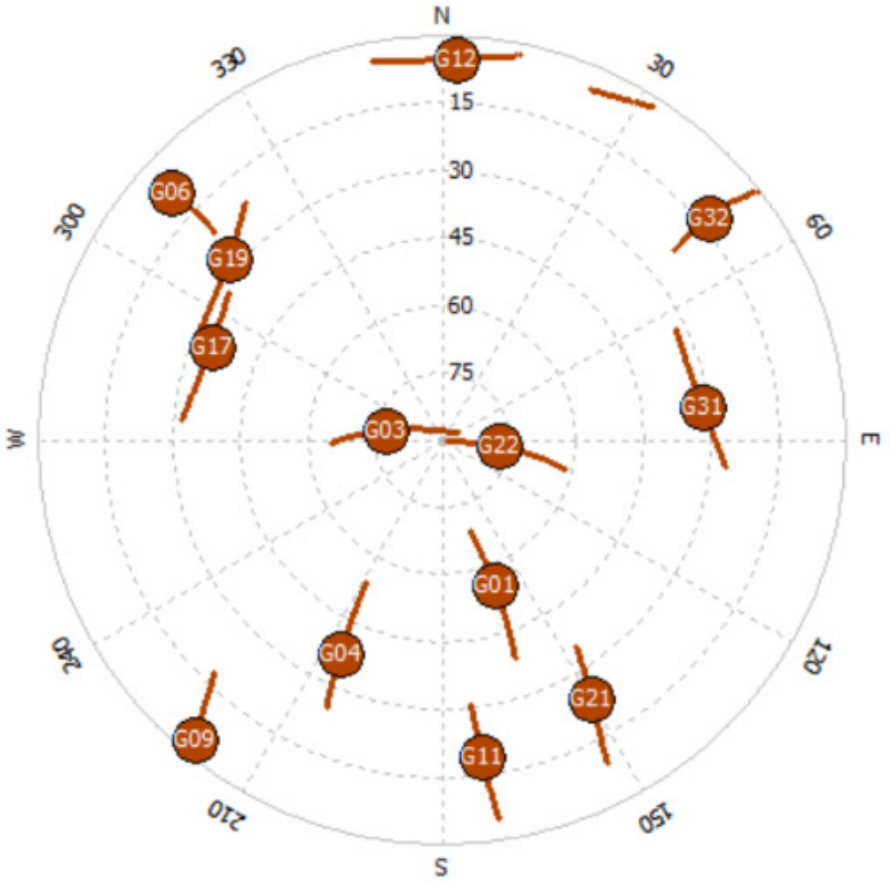


Figure 4. Skyplot of the GPS satellites during the experiment.

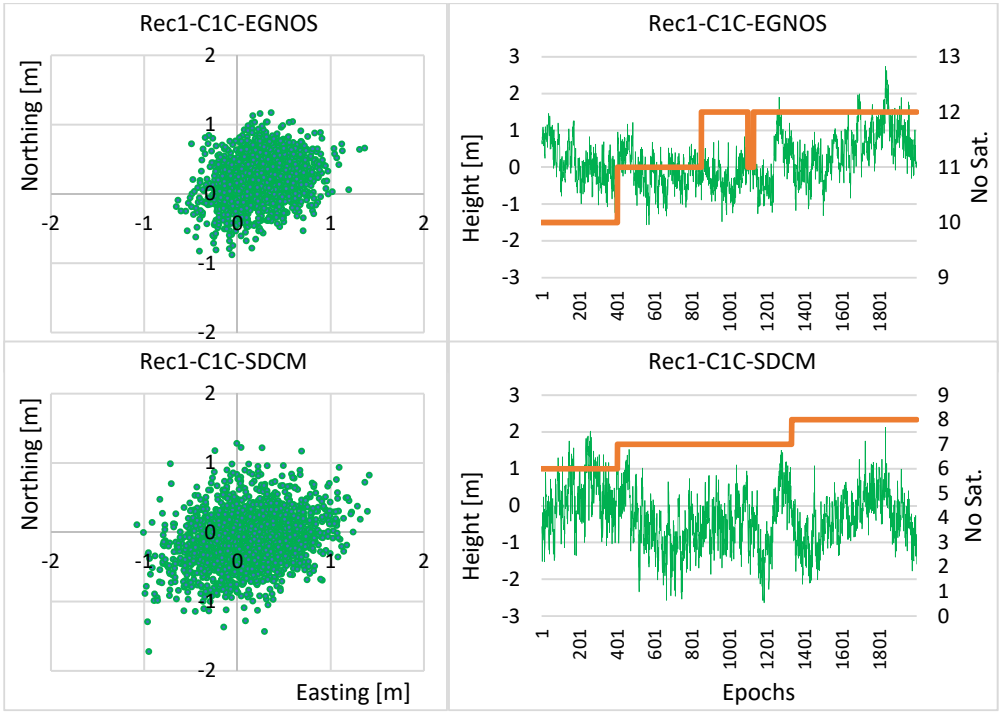


Figure 5. Real errors of horizontal and vertical coordinates of SBAS positioning based on C1C code, for the receiver Rec1 with EGNOS or SDCM corrections (Step II, see Figure 1).

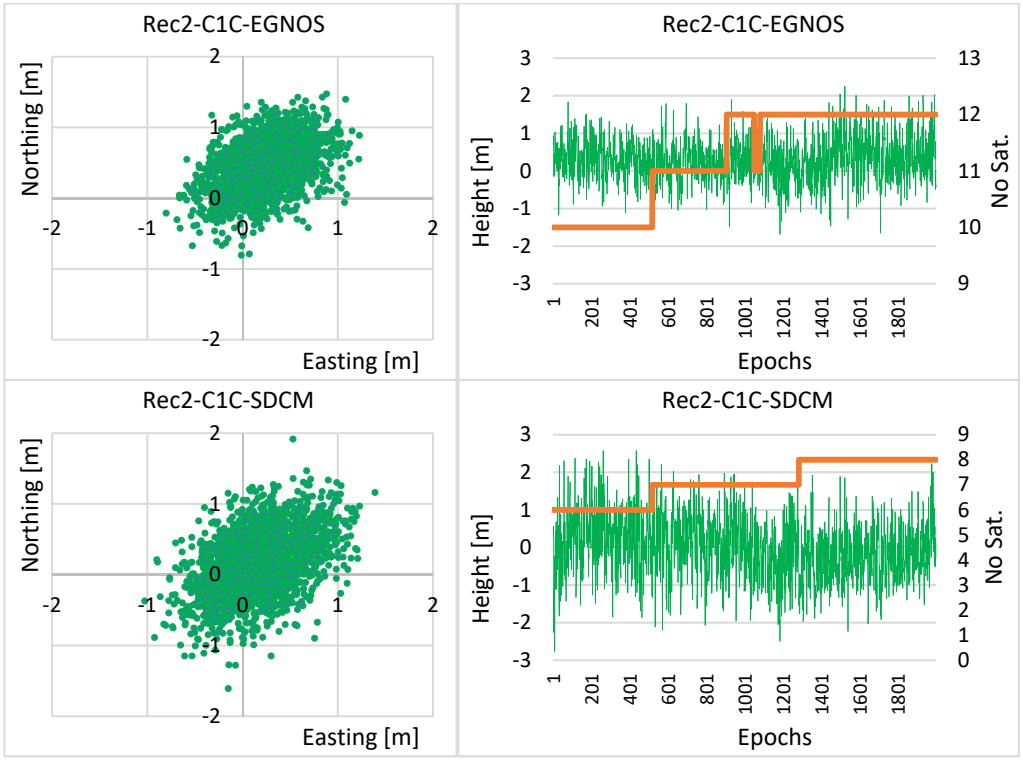


Figure 6. Real errors of horizontal and vertical coordinates of SBAS positioning based on C1C code, for the receiver Rec2 with EGNOS or SDCM corrections (Step II, see Figure 1).

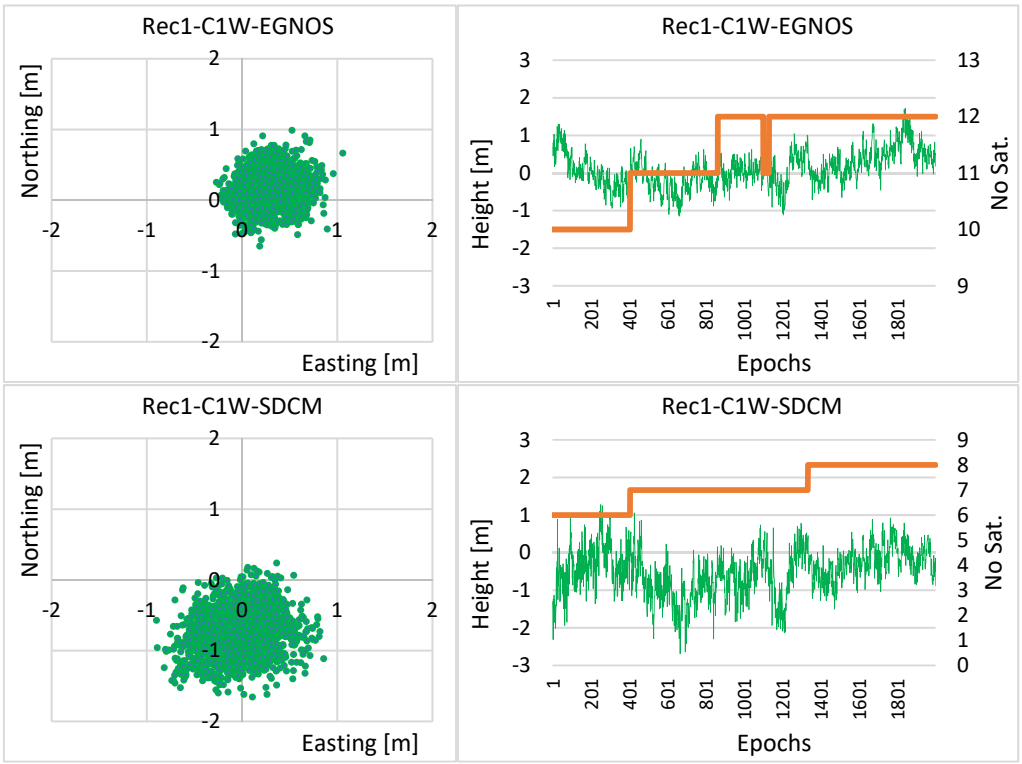


Figure 7. Real errors of horizontal and vertical coordinates of SBAS positioning based on C1W code, for the receiver Rec1 with EGNOS or SDCM corrections (Step II, see Figure 1).

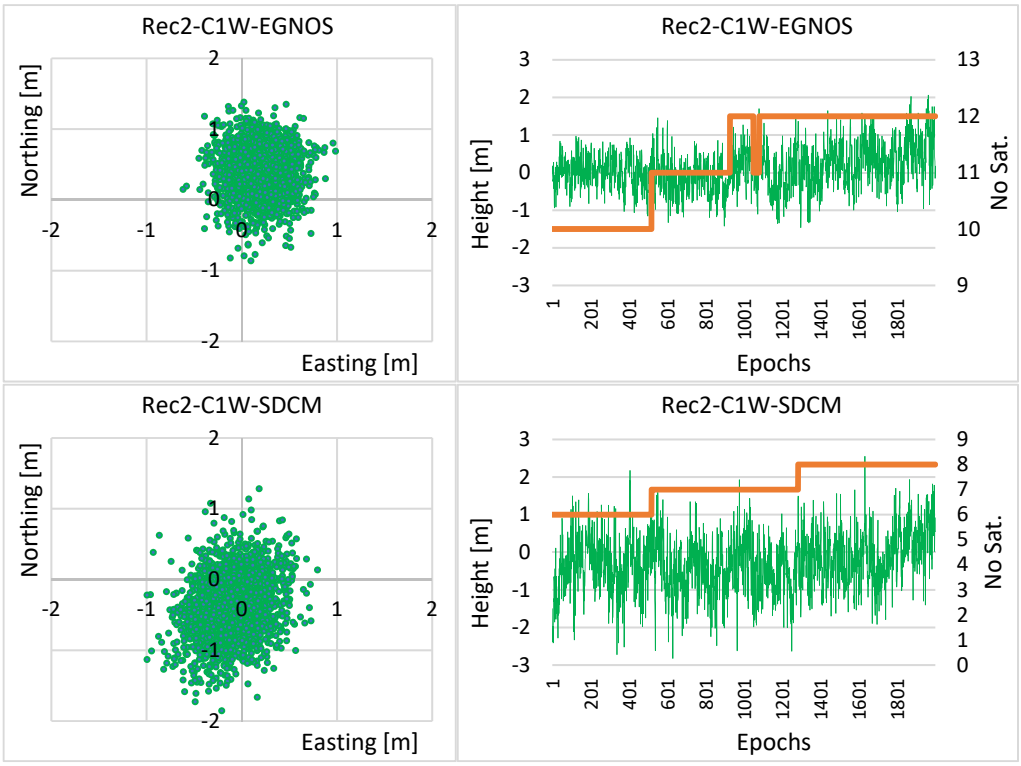


Figure 8. Real errors of horizontal and vertical coordinates of SBAS positioning based on C1W code, for the receiver Rec2 with EGNOS or SDCM corrections (Step II, see Figure 1).

Table 1. Average RMS errors for EGNOS and SDCM positioning, and C1C and C1W codes.

	LS	LS	LS
	RMS (*e*) (m)	**RMS (*n*) (m)**	**RMS (*h*) (m)**
R1-C1C-EGNOS	0.28	0.30	0.65
R1-C1C-SDCM	0.41	0.38	0.79
R2-C1C-EGNOS	0.33	0.54	0.62
R2-C1C-SDCM	0.38	0.45	0.82
R1-C1W-EGNOS	0.21	0.23	0.48
R1-C1W-SDCM	0.29	0.31	0.62
R2-C1W-EGNOS	0.22	0.34	0.55
R2-C1W-SDCM	0.27	0.42	0.77

Kalman filtering was next applied to the coordinates obtained from the RTKLIB calculations, significantly reducing the errors of the obtained positions in the individual measurement epochs. The real errors for the results using Kalman filtering for GPS/EGNOS and GPS/SDCM positions, for code C1C and C1W, are shown in Figures 9–12.

The average RMS errors for the coordinates n, e, h after Kalman filtering are shown in Table 2. The average RMS errors for the n, e, h coordinates equalled 0.37 m, 0.30 m, and 0.66 m, respectively. On the other hand, using additional Kalman filtering, the average standard deviation for the n, e, and h coordinates was 0.18 m, 0.18 m, and 0.38 m. The use of Kalman filtering resulted in a significant reduction in SBAS/EGNOS and SBAS/SDCM positioning errors. The horizontal components e and n were improved on average by around 39% and 47%, respectively, while the vertical component h improved its accuracy by around 41%.

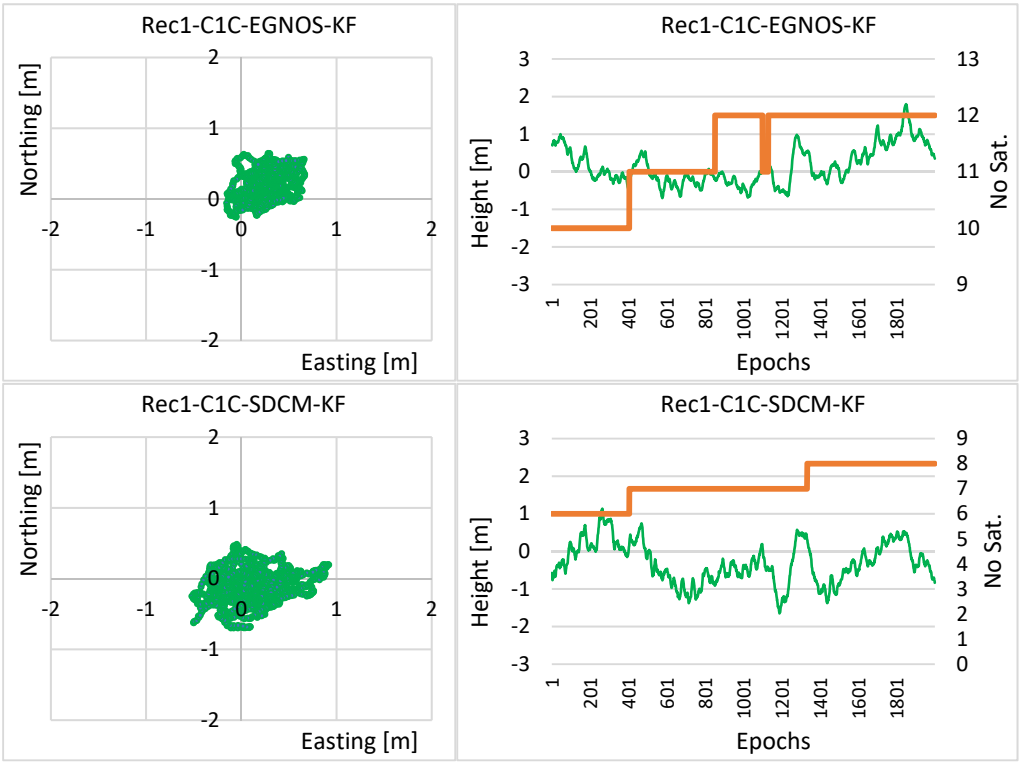


Figure 9. Real errors of horizontal and vertical coordinates of SBAS positioning based on C1C code, for the receiver Rec1 with EGNOS or SDCM corrections, with the use of Kalman filtering (Step III, see Figure 1).

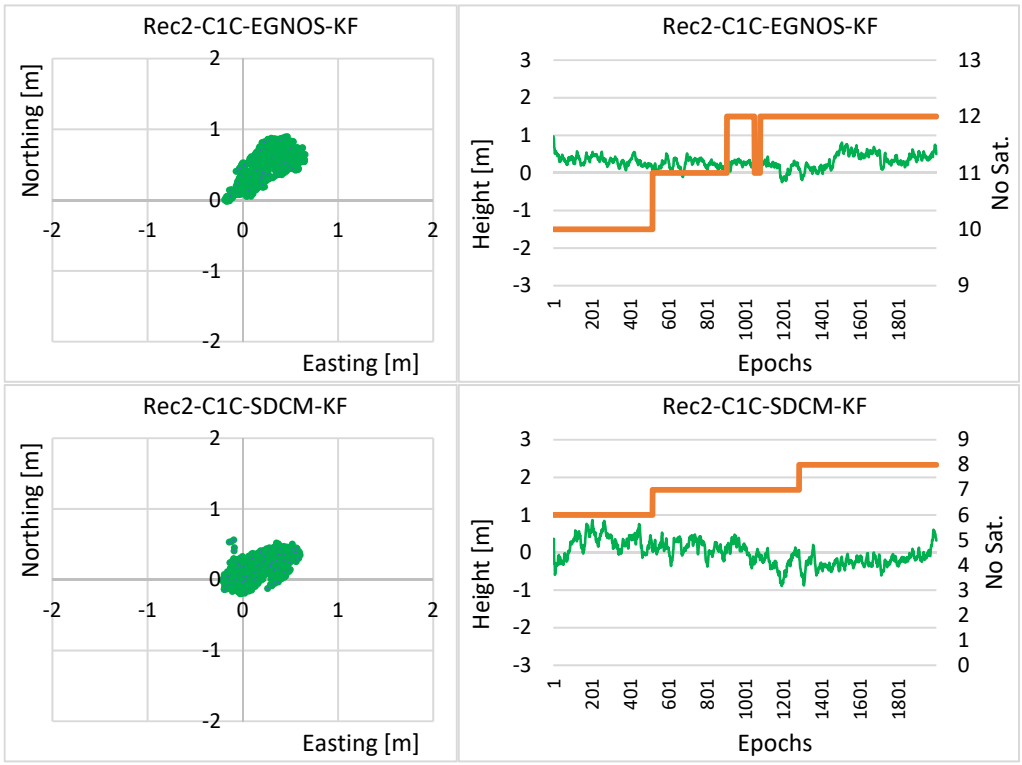


Figure 10. Real errors of horizontal and vertical coordinates of SBAS positioning based on C1C code, for the receiver Rec2 with EGNOS or SDCM corrections, with the use of Kalman filtering (Step III, see Figure 1).

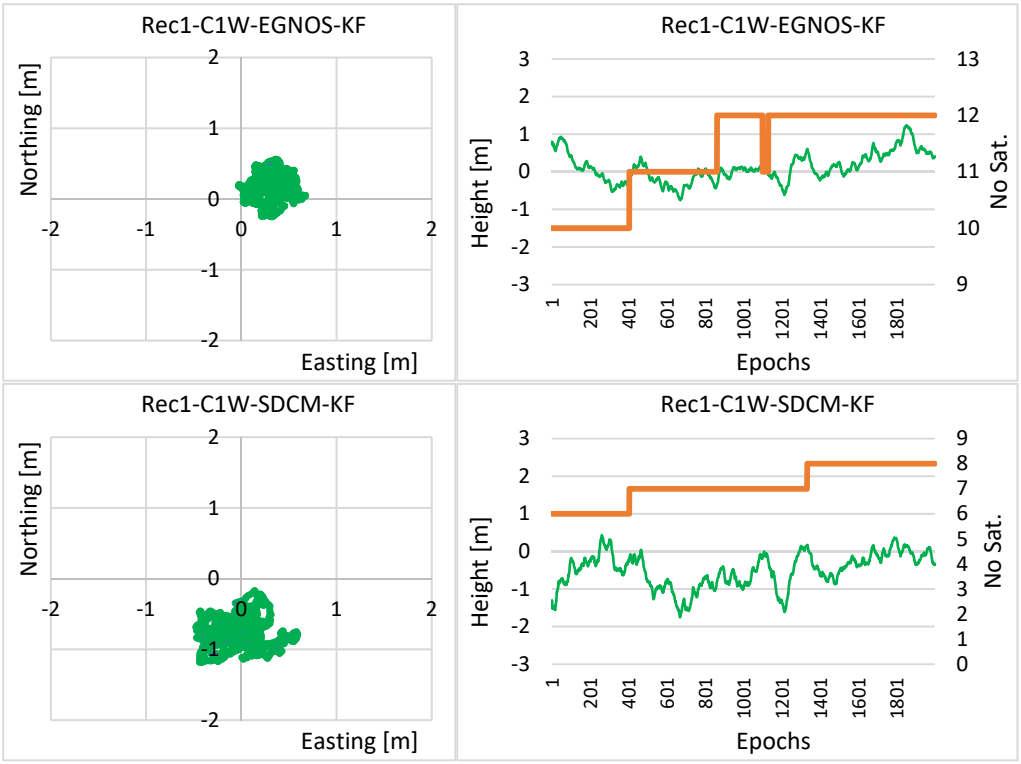


Figure 11. Real errors of horizontal and vertical coordinates of SBAS positioning based on C1W code, for the receiver Rec1 with EGNOS or SDCM corrections, with the use of Kalman filtering (Step III, see Figure 1).

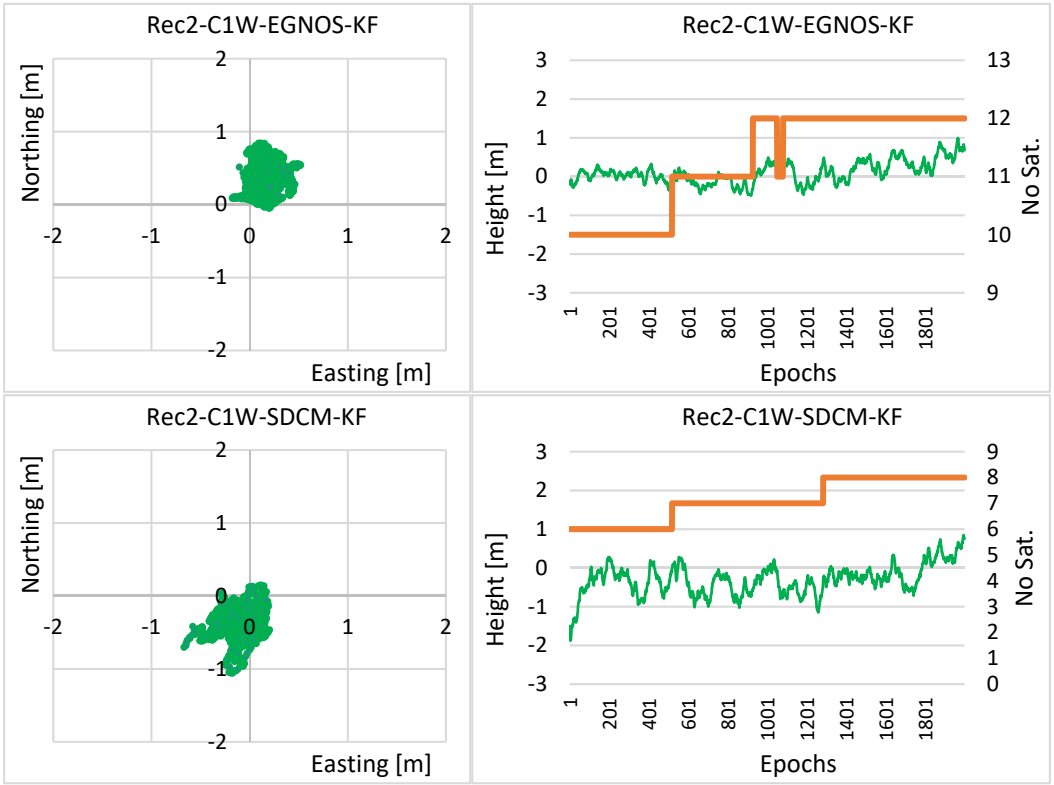


Figure 12. Real errors of horizontal and vertical coordinates of SBAS positioning based on C1W code, for the receiver Rec2 with EGNOS or SDCM corrections, with the use of Kalman filtering (Step III, see Figure 1).

Table 2. Average RMS errors for EGNOS and SDCM positioning as well as for codes C1C and C1W, additionally using Kalman filtering.

	LS+KF		LS+KF		LS+KF	
	RMS (*e*) (m)	**dRMS (%)**	**RMS (*n*) (m)**	**dRMS (%)**	**RMS (*h*) (m)**	**dRMS (%)**
R1-C1C-EGNOS	0.16	42	0.18	40	0.50	23
R1-C1C-SDCM	0.29	29	0.21	45	0.55	30
R2-C1C-EGNOS	0.18	45	0.20	63	0.17	72
R2-C1C-SDCM	0.18	52	0.15	67	0.32	61
R1-C1W-EGNOS	0.16	23	0.16	30	0.39	19
R1-C1W-SDCM	0.23	21	0.21	32	0.46	26
R2-C1W-EGNOS	0.11	50	0.19	44	0.28	49
R2-C1W-SDCM	0.14	48	0.18	57	0.39	49

The forced adjustment formulas were applied to the coordinates obtained from Kalman filtering, calculating the coordinates of the desired point P, which was located at the centre of the line between receivers *R*1 and *R*2. The findings of these calculations have been presented in Figures 13 and 14. The final coordinates averaged from EGNOS and SDCM calculations, obtained using C1C and C1W codes, are shown in Figure 15. Figure 13 shows real errors for EGNOS positioning, using C1C+C1W codes, while Figure 14 shows the real errors for SDCM positioning, also by means of C1C+C1W codes. The magnitudes of these errors are at a similar level for both horizontal and vertical components. However, it is clear that these errors are not correlated. For example, the horizontal component errors for EGNOS positioning are distributed in the north-eastern part (Figure 13), with respect to the true position, while for SDCM positioning, they are located below the reference coordinates (Figure 14). When comparing the error distribution for the vertical coordinate, one may also observe that there is no correlation between the EGNOS and the SDCM solutions. Moreover, it can be seen that the number of satellites for the EGNOS solution was higher than for the SDCM solution. This is probably due to the fact that the measurement was performed in Poland, i.e., outside the planned operation of the SDCM system. Hence, there is no SDCM correction for some satellites located low above the horizon. For EGNOS positioning and the two measurement codes C1C+C1W, the RMS errors were: 0.096 m (*e*), 0.121 m (*n*), 0.282 m (*h*), respectively, while for SDCM positioning, the RMS errors of the 3D positions were as follows: 0.156 m (*e*), 0.105 m (*n*), 0.308 m (*h*).

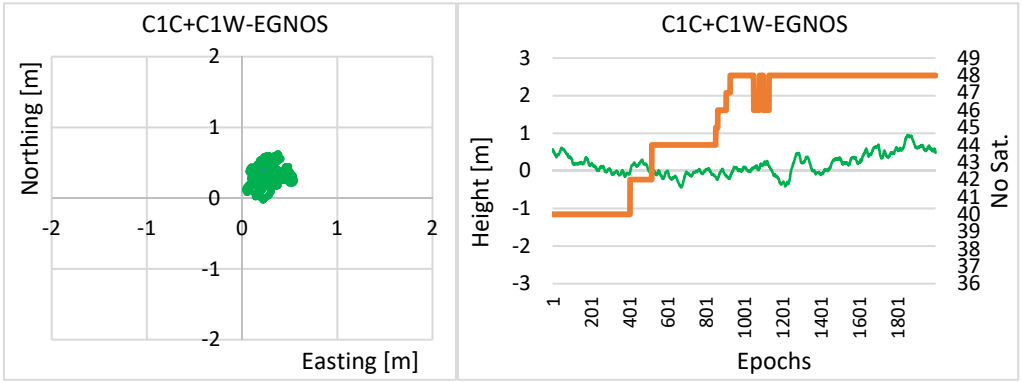


Figure 13. Real errors of coordinates of dual receiver in the constrained least squares adjustment of GPS/EGNOS positioning (Step IV, see Figure 1).

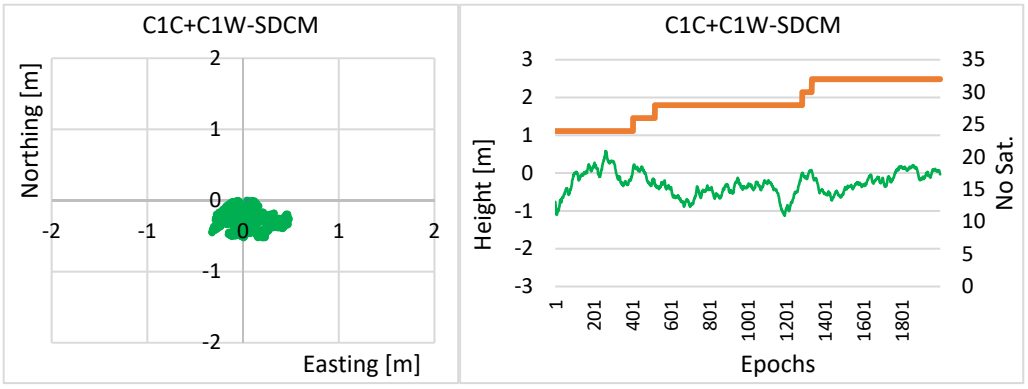


Figure 14. Real errors of coordinates of dual receiver in the constrained least squares adjustment of GPS/SDCM positioning (Step IV, see Figure 1).

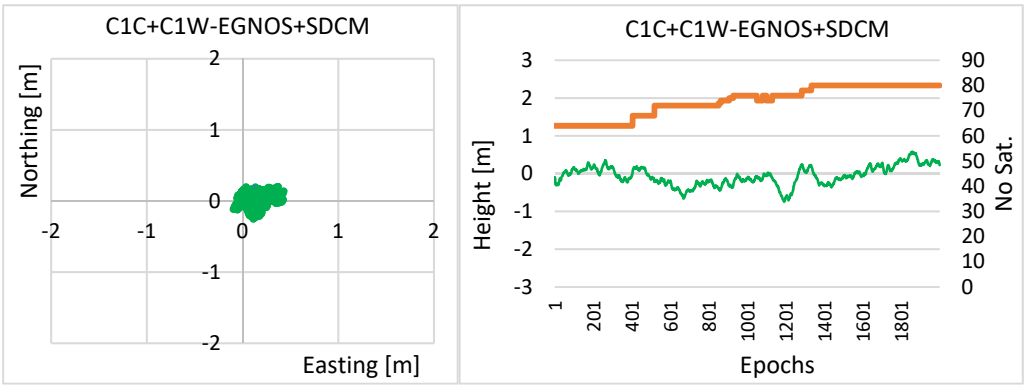


Figure 15. Real errors of finale coordinates of dual receiver GPS/(EGNOS+SDCM) positioning, with the use of C1C and C1W codes.

In the final solution (Figure 15), the coordinates obtained from the EGNOS system (C1C+C1W) were therefore averaged with the coordinates obtained from the SDCM system (C1C+C1W). The lack of correlation between these solutions resulted in a further increase in accuracy. The average RMS errors of 0.112 m and 0.079 m for the e and n coordinates, and 0.256 m for the vertical coordinate, were obtained. The real errors of the e, n, h coordinates ranged from −0.10 m to 0.43 m; −0.26 m to 0.20 m; −0.74 m to 0.57 m, respectively.

The EGNOS and SDCM corrections include atmospheric, satellite coordinates, and satellite clock corrections. When we use two different pseudo-ranges for C1C and C1W, the satellite differential code biases exist. These values are precisely estimated by the International GNSS service [60,61] (https://cddis.nasa.gov/archive/gnss/products/bias/, accessed on 20 June 2022), and for the satellites available in the experiment, these values were in the range (−1.47 ns–2.43 ns), as follows: G01 = −1.16 ns; G03 = −1.46 ns; G04 = −0.86 ns; G06 = −1.47 ns; G09 = −0.15 ns; G11 = 0.53 ns; G12 = −0.36 ns; G18 = −1.05 ns; G20 = 1.96 ns; G22 = 2.43 ns; G23 = −1.00 ns; G32 = −1.31 ns. However, differential code biases (DCB) in the RTKLIB software were not included. The average value of the DCB during the experiment was −0.33 ns, which gives us an average error of 0.1 m in pseudo-range measurements. Differential code biases also may exist in GNSS receivers [62]. These values seem to be specific for any GNSS receiver. Therefore, differential code biases should be analysed and included in multi-frequency SBAS positioning.

5. Accuracy Analysis

The accuracy analysis of the final positions was determined by the covariance matrix of the aligned results obtained from the constrained least squares adjustment [59]:

$$C_X = \sigma_0^2 Q_X \tag{28}$$

where

$$Q_X = \left(A^T PA\right)^{-1}\left(I_r - A_w^T[A_w\left(A^T PA\right)^{-1}A_w^T]^{-1}A_w\left(A^T PA\right)^{-1}\right) \tag{29}$$

$$I_r = A^T\left(A_w P^{-1}A_w^T\right)^{-1}A\left[A^T\left(A_w P^{-1}A_w^T\right)^{-1}A\right]^{-1} \tag{30}$$

$$\sigma_0^2 = \frac{V^T PV}{n + w - r} \tag{31}$$

n-number of observations, r-number of unknowns, w-number of conditions, i.e., $w = 1$.

The final coordinates are calculated from the Equation (27) and, therefore, the accuracy of the final coordinates is calculated from the covariance matrix (C_F) as follows:

$$C_F = D \times C_X \times D^T \tag{32}$$

where

$$D = \begin{bmatrix} 0.5 & 0 & 0 & 0.5 & 0 & 0 \\ 0 & 0.5 & 0 & 0 & 0.5 & 0 \\ 0 & 0 & 0.5 & 0 & 0 & 0.5 \end{bmatrix} \tag{33}$$

Taking into account the real errors of SBAS positioning and the confidence intervals, the coordinate values for a given probability (for the confidence level $1 - \alpha = 0.68$, i.e., for 1σ) should be within the interval:

$$P(Fmin < (e, n, h) < Fmax) = 1 - \alpha \tag{34}$$

Using the elements of the matrix C_F, it is possible to determine the confidence intervals for the 3D spatial coordinates:

$$Fmax = \sqrt{\sigma_N^2 + \sigma_E^2 + \sigma_h^2} = -Fmin \tag{35}$$

The $Fmin$ and $Fmax$ values for real positioning errors dE (dE = $e - e_{ref}$), dN (dN = $n - n_{ref}$), and dh (dh = $h - h_{ref}$) of EGNOS, SDCM, and EGNOS+SDCM, using two GNSS receivers and C1C+C1W observations at L1 (GPS) frequency, are shown in Figures 16–18.

In order to determine the efficiency of the SBAS positioning, the parameter $\Delta_{3D,SBAS}$, determined from the relationship, is as follows:

$$\Delta_{3D,SBAS} = \sqrt{(n_{SBAS} - n_{REF})^2 + (e_{SBAS} - e_{REF})^2 + (h_{SBAS} - h_{REF})^2} - \sqrt{\sigma_N^2 + \sigma_E^2 + \sigma_h^2} \tag{36}$$

The reliability of the developed model can, therefore, be assessed once the inequality has been satisfied:

$$\Delta_{3D,SBAS} \leq 0 \tag{37}$$

Measurement values $\Delta_{3D,EGNOS}$, $\Delta_{3D,SDCM}$, and $\Delta_{3D,EGNOS+SDCM}$ are shown in Figure 19. For the EGNOS system (Figure 16), only for 16 out of 2000 (0.008%) measurement epochs, the inequality expressed by Equation (37) was met. Consequently, the accuracy analysis determined by the covariance matrix was overly optimistic. For the SDCM system (Figure 17)—for 1181 out of 2000 (59%) epochs—the inequality was met, while for the EGNOS+SDCM solution (Figure 18)—1918 out of 2000 epochs satisfied the inequality, which was 95.9%. Thus, a combination of EGNOS and SDCM systems proved to be the most effective approach to increase accuracy and allow a more reliable determination of accuracy rather than using only one SBAS system.

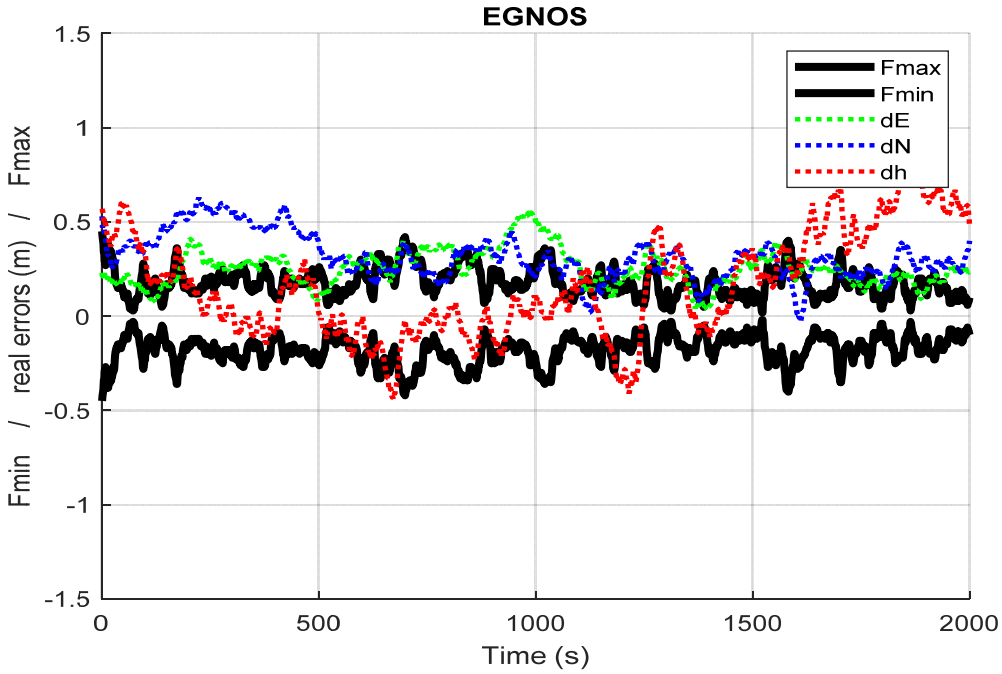


Figure 16. Confidence intervals for the calculated 3D error (*Fmin*; *Fmax*) with respect to the real horizontal and vertical errors, for the dual receiver EGNOS system and C1C+C1W codes.

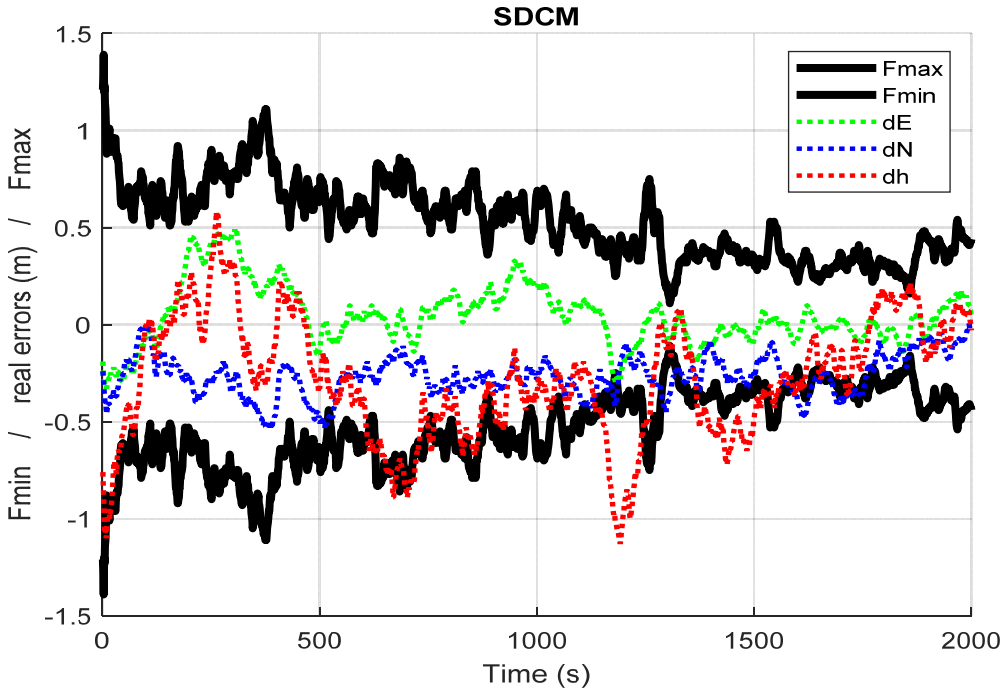


Figure 17. Confidence intervals for the calculated 3D error (*Fmin*; *Fmax*) with respect to the real horizontal and vertical errors, for the dual receiver SDCM system and C1C+C1W codes.

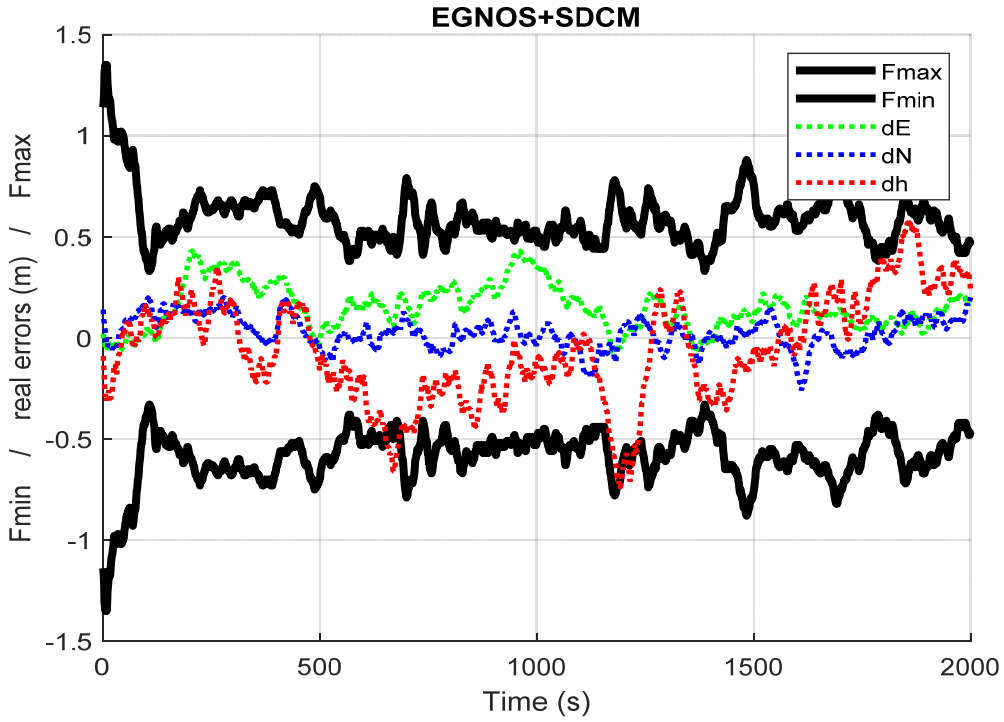


Figure 18. Confidence intervals for the calculated 3D error (*Fmin*; *Fmax*) with respect to the real horizontal and vertical errors, for the dual receiver EGNOS+SDCM and C1C+C1W codes.

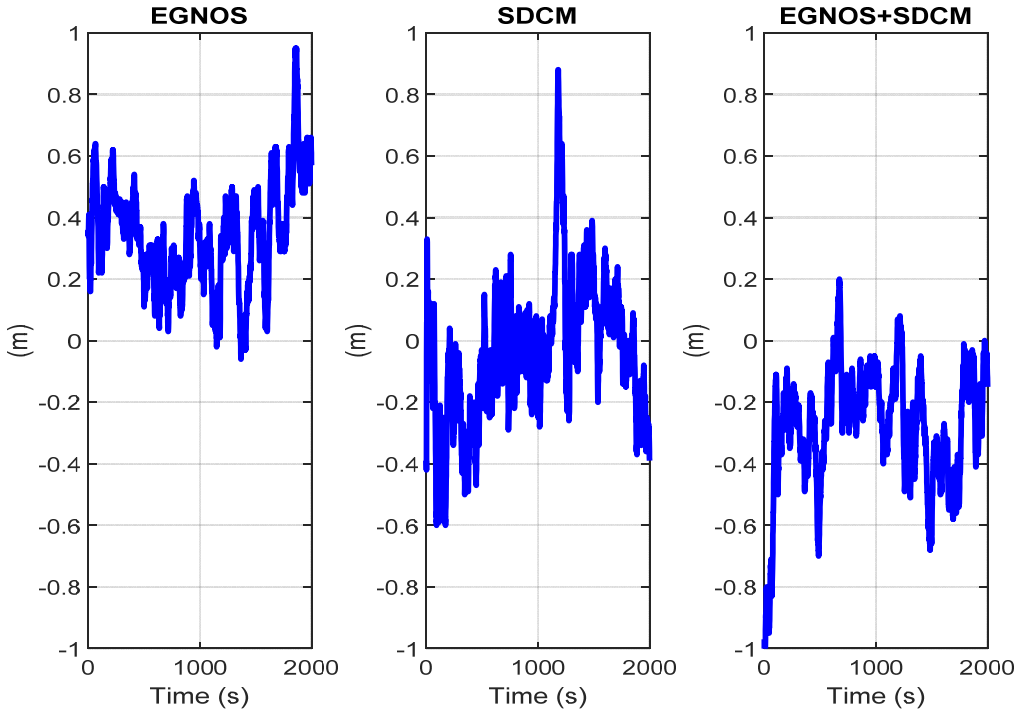


Figure 19. Validation of EGNOS, SDCM, and EGNOS+SDCM positioning based on the values $\Delta_{3D,SBAS}$ (see Equation (37)).

In the case of the EGNOS+SDCM solution, the value of the parameter was mainly below zero (Figure 19), which means that the simultaneous application of two EGNOS and SDCM systems enables a better accuracy analysis than in the case of applying only one EGNOS or SDCM system.

6. Conclusions

In general, SBAS positioning using EGNOS or SDCM uses the L1 frequency in the GPS and it is a civilian code C1C. However, some modern GNSS receivers also have a second code on the L1 frequency, the C1W code. Thus, it is possible to use both codes to improve the accuracy of SBAS positioning. This paper presents the calculations based on EGNOS and SDCM systems with the use of a Javad TRIUMPH-1 geodetic receiver. In addition, calculations were performed using a second Javad TRIUMPH-1 receiver at the same time. The two receivers, placed at a fixed distance, enable taking advantage of geometric conditions to be used to position the EGNOS+SDCM more accurately and to determine the confidence interval for the EGNOS+SDCM position with an assumed probability in a more reliable manner. This was achieved by applying Kalman filtering and least squares adjustment algorithms together with a condition of a constant spatial distance between the GNSS receivers. This significantly increased accuracy of EGNOS+SDCM positioning, achieving average RMS errors of approximately 0.15 m for horizontal coordinates and approximately 0.30 m for the vertical coordinate. The constrained least squares adjustment method enabled a more reliable accuracy determination for the EGNOS+SDCM solution rather than for a single EGNOS or SDCM system.

Author Contributions: Conceptualization, M.B. and K.K.; methodology, M.B.; software, M.B.; validation, K.K. and K.D.; formal analysis, M.B.; investigation, M.B. and K.K.; resources, M.B. and K.D.; data curation, M.B. and K.D.; writing—original draft preparation, M.B.; writing—review and editing, M.B. and K.D.; visualization, M.B.; supervision, M.B. and K.K.; project administration, M.B.; funding acquisition, K.K. All authors have read and agreed to the published version of the manuscript.

Funding: This research was funded by the Polish Air Force University.

Conflicts of Interest: The authors declare no conflict of interest.

References

1. Wubbena, G.; Bagge, A.; Seeber, G.; Boder, V.; Hankemeier, P. Reducing Distance Dependent Errors for Real-Time Precise DGPS Applications by Establishing Reference Station Networks. In Proceedings of the 9th International Technical Meeting of the Satellite Division of The Institute of Navigation (ION GPS 1996), Kansas City, MO, USA, 17–20 September 1996; pp. 1845–1852.
2. Weng, D.; Ji, S.; Lu, Y.; Chen, W.; Li, L. Improving DGNSS Performance through the Use of Network RTK Corrections. *Remote Sens.* **2021**, *13*, 1621. [CrossRef]
3. Bakuła, M.; Pelc-Mieczkowska, R.; Walawski, M. Reliable and redundant RTK positioning for applications in hard observational conditions. *Artif. Satell.* **2012**, *47*, 23–33. [CrossRef]
4. Bakuła, M.; Przestrzelski, P.; Kaźmierczak, R. Reliable Technology of Centimeter GPS/GLONASS Surveying in Forest Environments. *IEEE Trans. Geosci. Remote Sens.* **2015**, *53*, 1029–1038. [CrossRef]
5. Hernandez-Pajares, M.; Zornoza, J.M.J.; Subirana, J.S.; Farnworth, R.; Soley, S. EGNOS test bed ionospheric corrections under the October and November 2003 storms. *IEEE Trans. Geosci. Remote Sens.* **2005**, *43*, 2283–2293. [CrossRef]
6. Sieradzki, R.; Paziewski, J. Towards a reliable ionospheric polar patch climatology with ground-based GNSS. *IEEE Trans. Geosci. Remote Sens.* **2022**, *60*, 5802614. [CrossRef]
7. Gao, J. Integration of GPS with remote sensing and GIS: Reality and prospect. *Photogramm. Eng. Remote Sens.* **2002**, *68*, 447–454.
8. Lin, Y.C.; Manish, R.; Bullock, D.; Habib, A. Comparative Analysis of Different Mobile LiDAR Mapping Systems for Ditch Line Characterization. *Remote Sens.* **2021**, *13*, 2485. [CrossRef]
9. Li, T.; Zhang, H.; Gao, Z.; Niu, X.; El-Sheimy, N. Tight fusion of a monocular camera, MEMS-IMU, and single-frequency multi-GNSS RTK for precise navigation in GNSS-challenged environments. *Remote Sens.* **2019**, *11*, 610. [CrossRef]
10. Bar, Y.; Consoli, A.; Realini, E.; Caldera, S.; Mazzoni, A.; Crespi, M. Consumer GNSS chipsets-based, dual-frequency receivers as enablers of precise navigation and dense networks. *Meas. Sci. Technol.* **2019**, *30*, 044007.
11. Grayson, B.; Penna, N.T.; Mills, J.P.; Grant, D.S. GPS precise point positioning for UAV photogrammetry. *Photogramm. Rec.* **2018**, *33*, 427–447. [CrossRef]
12. Wang, J.; Xu, T.; Nie, W.; Xu, G. A new algorithm for a multi-baseline solution based on the equivalence principle. *Meas. Sci. Technol.* **2022**, *32*, 015015. [CrossRef]
13. Krasuski, K.; Ciećko, A.; Bakuła, M.; Wierzbicki, D. New strategy for improving the accuracy of aircraft positioning based on GPS SPP solution. *Sensors* **2022**, *20*, 4921. [CrossRef] [PubMed]
14. Krasuski, K.; Wierzbicki, D. Application the SBAS/EGNOS Corrections in UAV Positioning. *Energies* **2021**, *14*, 739. [CrossRef]
15. Ciećko, A.; Bakuła, M.; Grunwald, G.; Ćwiklak, J. Examination of Multi-Receiver GPS/EGNOS Positioning with Kalman Filtering and Validation Based on CORS Stations. *Sensors* **2020**, *20*, 2732. [CrossRef]

16. Paziewski, J. Precise GNSS single epoch positioning with multiple receiver configuration for medium-length baselines: Methodology and performance analysis. *Meas. Sci. Technol.* **2015**, *26*, 035002. [CrossRef]
17. Wilk, W.; Koc, W.; Specht, C.; Skibicki, J.; Judek, S.; Karwowski, K.; Chrostowski, P.; Szmagliński, J.; Dąbrowski, P.; Czaplewski, K.; et al. Innovative mobile method to determine railway track axis position in global coordinate system using position measurements performed with GNSS and fixed base of the measuring vehicle. *Measurement* **2021**, *175*, 109016. [CrossRef]
18. Li, M.; He, K.; Xu, T.; Lu, B. Robust adaptive filter for shipborne kinematic positioning and velocity determination during the Baltic Sea experiment. *GPS Solut.* **2018**, *22*, 81. [CrossRef]
19. Gao, F.; Xu, T.; Wang, N.; He, Y.; Luo, B. A shipborne experiment using a dual-antenna reflectometry system for GPS/BDS code delay measurements. *J. Geod.* **2020**, *94*, 88. [CrossRef]
20. Hong, C.K.; Park, C.H.; Han, J.H.; Kwon, J.H. Medium to long range kinematic GPS positioning with position-velocity-acceleration model using multiple reference stations. *Sensors* **2015**, *15*, 16895–16909. [CrossRef]
21. Wang, J.; Xu, T.; Nie, W.; Xu, G. GPS/BDS RTK Positioning Based on Equivalence Principle Using Multiple Reference Stations. *Remote Sens.* **2020**, *12*, 3178. [CrossRef]
22. Wang, J.; Xu, T.; Nie, W.; Xu, G. A simplified processing algorithm for multi-baseline RTK positioning in urban environments. *Measurement* **2021**, *179*, 109446. [CrossRef]
23. Bakuła, M.; Kaźmierczak, R. Technology of rapid and ultrarapid static GPS/GLONASS surveying in urban environments. In Proceedings of the 2017 Baltic Geodetic Congress (BGC Geomatics) IEEE, Gdansk, Poland, 22–25 June 2017; pp. 336–342.
24. Bakuła, M. Constrained and network multi-receiver single-epoch RTK positioning. *Surv. Rev.* **2020**, *52*, 289–298. [CrossRef]
25. Loh, R.; Wullschleger, V.; Elrod, B.; Lage, M.; Haas, F. The US Wide-Area Augmentation System (WAAS). *Navigation* **1995**, *42*, 435–465. [CrossRef]
26. Walter, T.; Kee, C.; Chao, Y.C.; Tsai, Y.J.; Peled, U.; Ceva, J.; Barrows, A.K.; Abbott, E.; Powell, D.; Enge, P.; et al. Flight Trials of the Wide Area Augmentation System (WAAS). In Proceedings of the ION GPS-94 7th International Technical Meeting of the Satellite Division of the Institute of Navigation, Salt Palace Convention Center, Salt Lake City, UT, USA, 20–23 September 1994; pp. 1537–1546.
27. Bolstad, P.; Jenks, A.; Berkin, J.; Horne, K.; Reading, W.H. A comparison of autonomous, WAAS, real-time, and post-processed global positioning systems (GPS) accuracies in northern forests. *North J. Appl. For.* **2005**, *22*, 5–11. [CrossRef]
28. Radio Technical Committee for Aeronautics (RTCA). *Minimum Operational Performance Standards for Airborne Equipment Using Global Positioning System/Wide Area Augmentation System*; Doc. DO-229D, with Change 1, 2013; Radio Technical Committee for Aeronautics (RTCA): Washington, DC, USA, 2006.
29. Shimamura, A. MSAS (MTSAT satellite-based augmentation system) project status. *Air Space Eur.* **1999**, *2*, 63–67. [CrossRef]
30. Liu, Y.; Cao, Y.; Tang, C.; Chen, J.; Zhao, L.; Zhou, S.; Hu, X.; Tian, Q.; Yang, Y. Pseudorange Bias Analysis and Preliminary Service Performance Evaluation of BDSBA. *Remote Sens.* **2021**, *13*, 4815. [CrossRef]
31. Choy, S.; Kuckartz, J.; Dempster, A.G.; Rizos, C.; Higgins, M. GNSS satellite-based augmentation systems for Australia. *GPS Solut.* **2017**, *21*, 835–848. [CrossRef]
32. European GNSS Agency (GSA). *EGNOS Open Service (OS) Service Definition Document (v. 2.3)*; The European GNSS Agency: Prague, Czech Republic, 2017.
33. Averin, S.; Dvorkin, V.; Karutin, S.; Kurshin, V.; Urlichich, U.; Klimov, V. Russian System for Differential Correction and Monitoring: A Concept and Results of the First Phase of Development. In Proceedings of the 19th International Technical Meeting of the Satellite Division of The Institute of Navigation (ION GNSS 2006), Fort Worth, TX, USA, 26–29 September 2006; pp. 2103–2110.
34. Averin, S.V.; Dvorkin, V.V.; Karutin, V.S.N.; Sergey, N. Russian System for Differential Correction and Monitoring: A Concept, Present Status, And Prospects For Future. In Proceedings of the 20th International Technical Meeting of the Satellite Division of The Institute of Navigation (ION GNSS 2007), Fort Worth, TX, USA, 25–28 September 2007; pp. 3037–3044.
35. Ali, K.; Pini, M.; Dovis, F. Measured performance of the application of EGNOS in the road traffic sector. *GPS Solut.* **2012**, *16*, 135–145. [CrossRef]
36. Skórkowski, A.; Topór-Kamiński, T. Analysis of EGNOS-augmented GPS receiver positioning accuracy. *Acta Phys. Pol.* **2012**, *122*, 821–824. [CrossRef]
37. Konin, V.; Shyshkov, F. Extending the reach of SBAS. Some aspects of EGNOS performance in Ukraine. *Inside GNSS* **2015**, *1*, 50–54.
38. Grunwald, G.; Bakuła, M.; Ciećko, A. Study of EGNOS accuracy and integrity in eastern Poland. *Aeronaut. J.* **2016**, *120*, 1275–1290. [CrossRef]
39. Grunwald, G.; Bakuła, M.; Ciećko, A.; Kaźmierczak, R. Examination of GPS/EGNOS integrity in north-eastern Poland. *IET Radar Sonar Navig.* **2016**, *10*, 114–121. [CrossRef]
40. Specht, C.; Pawelski, J.; Smolarek, L.; Specht, M.; Dąbrowski, P.S. Assessment of the positioning accuracy of DGPS and EGNOS systems in the Bay of Gdansk using maritime dynamic measurements. *J. Navig.* **2019**, *72*, 575–587. [CrossRef]
41. GSA. *EGNOS Safety of Life (SoL) Service Definition Document (v. 3.3)*; The European GNSS Agency: Prague, Czech Republic, 2019.
42. Krasuski, K. Application of the GPS/EGNOS solution for the precise positioning of an aircraft vehicle. *Sci. J. Sil. Univ. Technol. Ser. Transp.* **2017**, *96*, 81–93. [CrossRef]
43. Krasuski, K.; Ciećko, A.; Grunwald, G.; Wierzbicki, D. Assessment of velocity accuracy of aircraft in the dynamic tests using GNSS sensors. *Facta Univ. Ser. Mech. Eng.* **2020**, *18*, 301–313. [CrossRef]

44. Kirschenstein, M.; Krasuski, K.; Goś, A. Methods of precise aircraft positioning in the GPS system with an application of the troposphere correction. *Sci. J. Sil. Univ. Technol.* **2020**, *109*, 73–84. [CrossRef]
45. Krasuski, K.; Wierzbicki, D. Monitoring aircraft position using EGNOS data for the SBAS APV approach to the landing procedure. *Sensors* **2020**, *20*, 1945. [CrossRef]
46. Lim, C.; Park, B.; So, H.; Jang, J.; Seo, S.; Park, J.; Bu, S.; Lee, C. Analysis on the multi-constellation SBAS performance of SDCM in Korea. *J. Position. Navig. Timing* **2016**, *5*, 181–191. [CrossRef]
47. Park, K.W.; Cho, M.; Park, C. An efficient positioning method for multi-GNSS with multi-SBAS. *J. Position. Navig. Timing* **2018**, *7*, 245–253.
48. Park, K.W.; Park, J.I.; Park, C. Efficient methods of utilizing multi-SBAS corrections in multi-GNSS positioning. *Sensors* **2020**, *20*, 256. [CrossRef]
49. Krasuski, K.; Wierzbicki, D.; Bakuła, M. Improvement of UAV Positioning Performance Based on EGNOS+SDCM Solution. *Remote Sens.* **2021**, *13*, 2597. [CrossRef]
50. Weng, D.; Chen, W. SBAS enhancement using an independent monitor station in a local area. *GPS Solut.* **2019**, *23*, 12. [CrossRef]
51. Zhang, Y.; Xiao, Z.; Liu, Z.; Tang, X.; Ou, G. SBAS performance improvement with a new under sampled ionosphere threat model based on relative coverage metric. *J. Atmos. Sol.-Terr. Phys.* **2020**, *198*, 105178. [CrossRef]
52. Romero, I. RINEX The Receiver Independent Exchange Format Version 3.05. ESA/ESOC/Navigation Support Office. 2020. Available online: https://files.igs.org/pub/data/format/rinex305.pdf (accessed on 1 May 2022).
53. Kaplan, E. *Understanding GPS/GNSS: Principles and Applications*, 2nd ed.; Artech House: Norwood, MA, USA, 2006.
54. Takasu, T. RTKLIB ver. 2.4.2 Manual, RTKLIB: An Open Source Program, Package for GNSS Positioning. 2013. Available online: http://www.rtklib.com/prog/manual_2.4.2.pdf (accessed on 10 February 2022).
55. Minkler, G.; Minkler, J. *Theory and Applications of Kalman Filtering*; Magellan Book Company: Bamberg, Germany, 1993.
56. Brown, R.G.; Hwang, P.Y. *Introduction to Random Signals and Applied Kalman Filtering: With MATLAB Exercises and Solutions*; Wiley: Hoboken, NJ, USA, 1997.
57. Kayton, M.; Fried, W.R. *Avionics Navigation Systems*; John Wiley & Sons: Hoboken, NJ, USA, 1997.
58. Baran, L.W. *Teoretyczne Podstawy Opracowania Wyników Pomiarów Geodezyjnych*; Wydawnictwo Naukowe PWN: Warsaw, Poland, 1999.
59. Wiśniewski, Z. *Rachunek Wyrównawczy w Geodezji (Z Przykładami)*; Wydawnictwo UWM: Olsztyn, Poland, 2005.
60. Montenbruck, O.; Hauschild, A.; Steigenberger, P. Differential code bias estimation using multi-GNSS observations and global ionosphere maps. *Navig. J. Inst. Navig.* **2014**, *61*, 191–201. [CrossRef]
61. Wang, N.; Yuan, Y.; Li, Z.; Montenbruck, O.; Tan, B. Determination of differential code biases with multi-GNSS observations. *J. Geod.* **2016**, *90*, 209–228. [CrossRef]
62. Zhang, B.; Zhao, C.; Odolinski, R.; Liu, T. Functional model modification of precise point positioning considering the time-varying code biases of a receiver. *Satell. Navig.* **2021**, *2*, 11. [CrossRef]